

B. Development of Materials Analysis Tools for Studying NO_x Adsorber Catalysts (CRADA No. ORNL-02-0659 with Cummins, Inc.)

Thomas Watkins, Larry Allard, Doug Blom, Michael Lance, and Harry Meyer
Oak Ridge National Laboratory
P.O. Box 2008
Oak Ridge, TN 37831-6064
(865) 574-2046; fax: (865) 574-3940; e-mail: watkinstr@ornl.gov

DOE Technology Development Area Specialist: James J. Eberhardt
(202) 586-9837; fax: (202) 586-1600; e-mail: james.eberhardt@ee.doe.gov
ORNL Technical Advisor: D. Ray Johnson
(865) 576-6832; fax: (865) 574-6098; e-mail: johnsondr@ornl.gov

Contractor: Oak Ridge National Laboratory, Oak Ridge, Tennessee
Contract No.: DE-AC05-00OR22725

Objective

- Produce a quantitative understanding of the processing and in-service effects on NO_x adsorber catalyst technology leading to an exhaust aftertreatment system with improved catalyst performance capable of meeting the 2007 emission requirements.

Approach

- Characterize lab-engine tested samples with X-ray diffraction (XRD), spectroscopy, and microscopy.
- Correlate findings with Cummins data and experience.

Accomplishments

- Evaluated gradient formation on a macro scale of active elements on a catalyst as a function of catalyst history and operating conditions.
- Supported continued characterizations of new materials from various stages of the catalyst's life cycle.
- Begun determination of the soot and ash distribution as a function of macroscopic position within the NSR catalyst support brick.

Future Direction

- Evaluation of thermal degradation of a NO_x stoichiometric ratio (NSR) catalyst as a function of macroscopic position within the catalyst support brick.
- Continue the determination of the soot and ash distribution as a function of macroscopic position within the NSR catalyst support brick.

Introduction

To meet the 2007 emission requirements for diesel exhaust, aftertreatment in diesel engines may be necessary. The technology necessary for 2007

will need to integrate aftertreatment with engine control systems. Currently, no commercial off-the-shelf technologies are available to meet these standards. Consequently, Cummins, Inc. is working to understand the basic science necessary to

effectively utilize these catalyst systems. Oak Ridge National Laboratory (ORNL) is assisting with the materials characterization effort.

Base metal oxides (BMOs) are major components in current SO_x and NO_x adsorbers that Cummins seeks to use in NO_x adsorber catalyst systems. The function of these adsorbers is to collect oxy-sulfur (SO_x) and surface nitrite/nitrate (NO_x) species. These species are to be released from these surface sites during regeneration, where the adsorber BMO is either heated to some critical temperature or exposed to a reducing or reactant atmosphere. Sulfur poisoning of adsorber catalysts is a major problem that must be resolved for BMO-based emission reduction technologies to become commercially viable.

Approach

In general, the crystal structure, morphology, phase distribution, particle size, and surface species of catalytically active materials supplied by Cummins will be characterized using XRD, Raman spectroscopy, and electron microscopy. These materials will come from all stages of the catalyst's life cycle: raw materials, as-calcined, sulfated, regenerated, etc. Both ORNL and Cummins personnel have participated in this work.

Samples

Briefly, Cummins provided various series of "core" samples taken from cordierite "bricks" containing platinum, γ -alumina and BaCO_3 or platinum and γ -alumina. The general features of each series will be given below in the text as needed. The brick/core samples consisted of a series with varied amounts of platinum loading, a sample that had lost performance after numerous desulfations, and a sample loaded with sulfur.

Results

The following is a summary of the work from October 2004 to September 2005.

X-ray

X-ray diffraction (XRD) was employed to understand the crystalline nature of the samples. For the unfamiliar, the following analogy can be applied:

As a fingerprint identifies a person, so a diffraction pattern identifies a crystalline material.

A model system was analyzed and consisted of platinum particles dispersed on a γ -alumina (Al_2O_3) on a cordierite ($\text{Mg}_2\text{Al}_4\text{Si}_5\text{O}_{18}$, the core/brick material) substrate. This series of samples were "redoxed pulsed" to remove nitrogen from the oxidation catalyst. Here, redox pulsing entails going from a rich/reducing fuel mixture to a lean/oxidizing fuel mixture and back. Samples A, B, C and D were designated the baseline, 6 h at 350°C , 6 hours at 350°C -low volume, and 6 h at 450°C , respectively. The conditions for sample D were regarded as the most severe and would be the most likely to cause Pt crystallite growth. Figure 1 compares the XRD pattern of sample D to the as-received γ -alumina powder. The powder has a high surface area, and the very broad peaks of the powder indicate a small crystallite size, 3 nm. A crystallite is a region of coherent diffraction and can be thought of as a sub-grain, which is a very small perfect crystal. The narrower alumina peaks of sample D, indicate that the crystallite size has increased and that the surface area has likely decreased. Figure 2 shows that the γ -alumina has transformed to θ -alumina and indicates that sample has experienced temperatures in the 727 to 1027°C range.¹ Note the platinum and θ -alumina superimpose. Figure 3(a) shows the experimental set-up used to collect platinum crystallite information as a function of macroscopic length along the sample. As was inferred above, the x-ray crystallite size is related to the x-ray peak broadening. Typically, the size of a crystallite is smaller than the grain size of a material as observed on the scanning electron microscopy (SEM). Significant contributions to x-ray peak broadening occur when the crystallite size is less than 100 nm. The lower bound is approximately 2 nm. Figure 3 shows the crystallite size data for samples A, B, C, and D. The crystallite size did not vary systematically along the length. As will be shown later, the size does not agree with that found in the microscopy section. This is likely due to the aforementioned peak superposition. Thus, the crystallite sizes given may more accurately reflect the size of the θ -alumina.

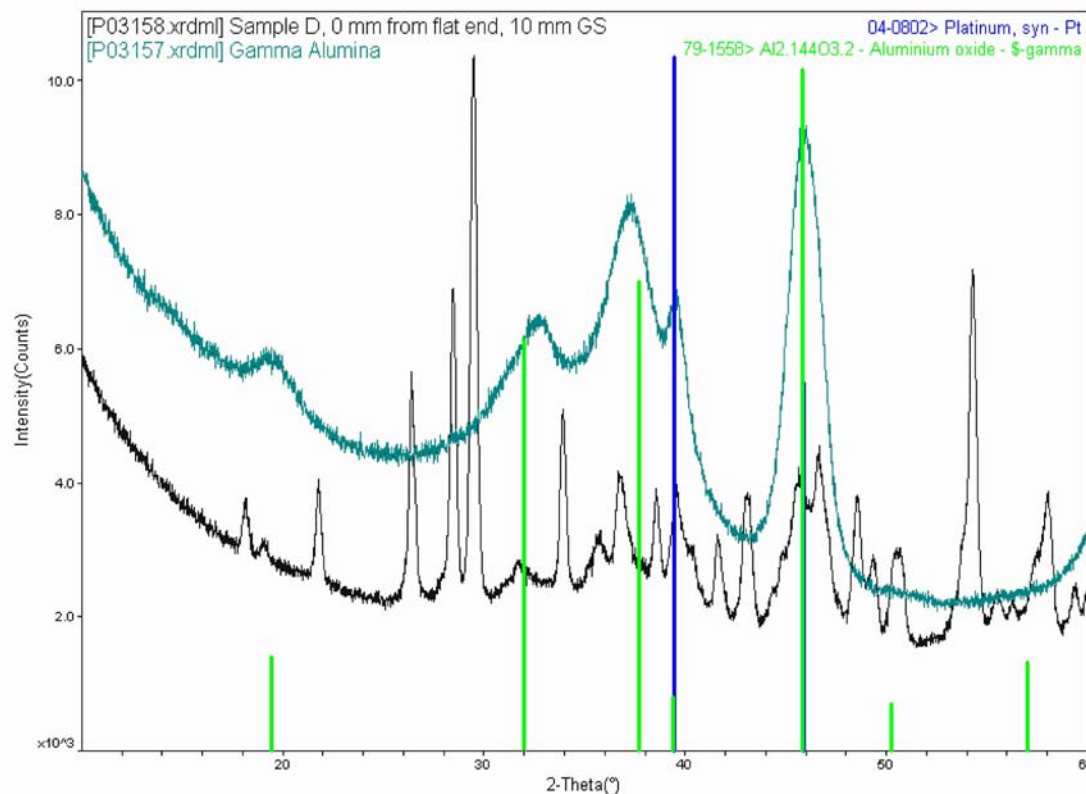


Figure 1. The diffraction patterns for the as-received γ -alumina powder and sample D (redox pulsed for 6 h at 450°C).

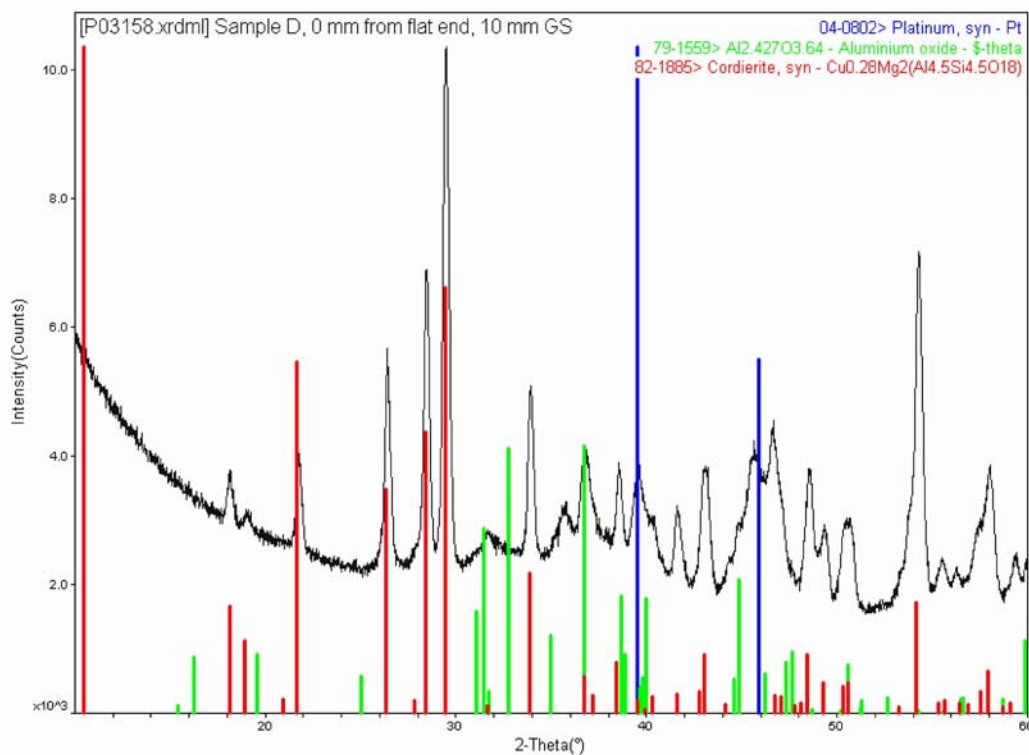
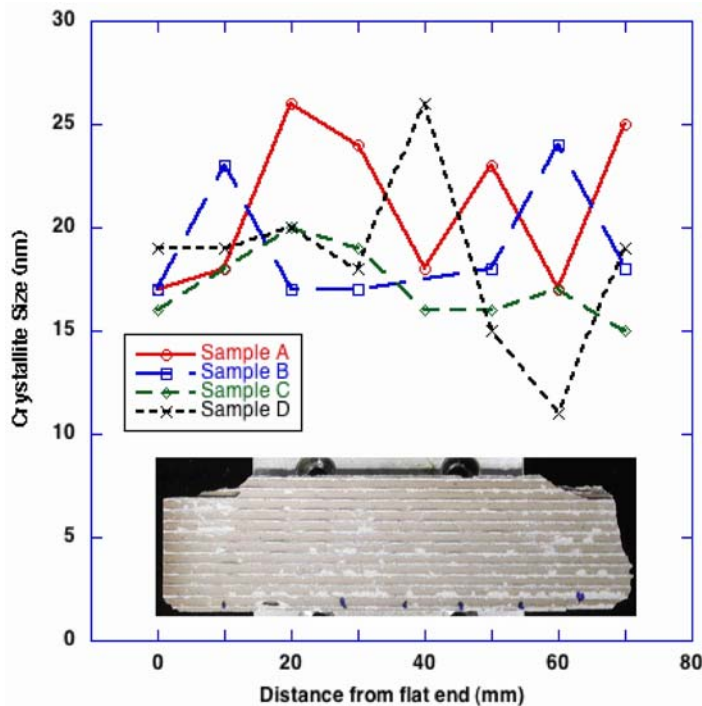


Figure 2. The diffraction pattern for sample D (redox pulsed for 6 h at 450°C).



Sample
Silicon wafer masks

(a)



(b)

Figure 3. (a) Silicon wafer masks allow measurement of data every 10 mm. (b) Platinum/alumina crystallite size as a function of length along the sample.

Raman Spectroscopy

Raman spectroscopy measures the characteristic vibrational energy levels of molecules and crystals and so is very sensitive to any changes in bonding, stoichiometry, and phase/symmetry.

Soot oxidation has been a critical issue for regeneration of diesel particulate filters (DPFs). The design of the regeneration strategy and the durability requirement for DPFs depend on an understanding of soot burning. Raman spectroscopy has been used to monitor surface configuration changes. Under thermal aging, engine soot undergoes a transformation from a mostly amorphous carbon structure into more orderly polyaromatic structures, which exhibit resistance toward oxidation. Certain neutralization products, such as thio-phosphorous and phosphorous derivatives, can also alter the thermal behavior of soot through interactions between ash- and soot-adsorbed species. The incomplete regeneration can be attributed to a buildup of a physical barrier that prevents oxygen and/or NO₂ from diffusing effectively onto the carbon surface.

Raman spectroscopy offers a unique way to characterize the long-range interactions and the order-disorder effects on carbonaceous materials. Both the first and the second-order features can be seen with Raman. Pristine graphite crystals show two first-order Raman features located at 42 and 1578 cm⁻¹. The 1578 cm⁻¹ band, with a full width at half-maximum bandwidth of 16 cm⁻¹ (see Figure 4), is referred to as the graphitic band (G). Grinding the graphite crystal generates an additional band at 1335 cm⁻¹, which can be assigned as the disordered band (D). Additional grinding gives an increase in the intensity and bandwidth of the disordered band. The appearance of the disordered band can be attributed to the disorder relaxation where the wave-vector selection rules are broken by lattice discontinuities and structural defects.

The Raman spectra of the fresh and the artificially matured samples of AIC are shown in Figure 4. After heating at 950°C, additional bands begin to show around 680 ~ 1000 cm⁻¹, which can be assigned to metal oxides. When samples are heated at high temperatures, spectral interference

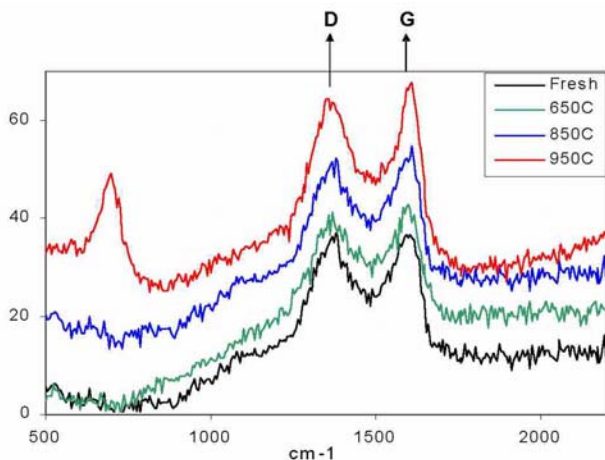


Figure 4. Raman spectra of A1C engine soot aged at various temperatures.

from ash components with the carbon bands begins to become pronounced. As the maturation temperature is increased, the graphitic band becomes sharper, and the intensity is enhanced. The transition frequency of the disordered band is also shifted to a slightly lower frequency. Similar trends are also seen in other samples. All these spectral trends suggest a structural change of the sample during thermal maturation.

The frequency ratios of the graphitic to disorder peak ($R = f_G/f_D$) measured for all three samples are plotted in Figure 5. All three samples follow a general trend with an increase of R with the maturation temperature. The increase of R for soot maturation is from 0.37 (<650°C) to 0.48 (>850°C). The change shows little statistical significance at temperatures

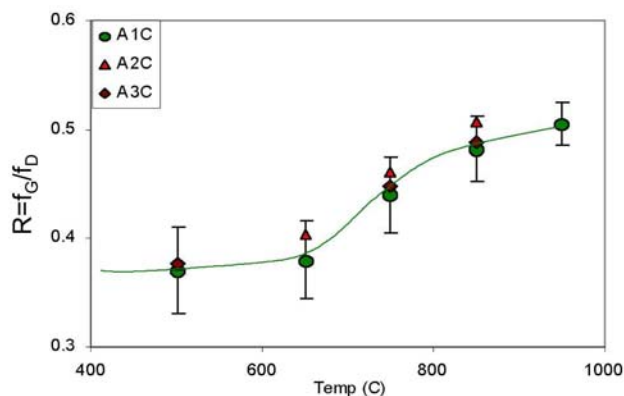


Figure 5. The correlation between Raman band ratio ($R = f_G/f_D$) and temperature.

below 700°C. Above 750°C, a rapid enhancement is observed, and the curve levels off beyond 850°C. The major change seems to occur around 700°C. This temperature is consistent with most young coal samples where their maturation scale changes dramatically under artificial pyrolysis around 700°C. This result shows that Raman spectroscopy can be used to monitor the degree of long-range order in soot samples, which is a key parameter in determining the regeneration processing of DPFs. More research is planned to better understand the kinetics of soot burning and DPF aging.

Microscopy

Scanning transmission electron microscopy (STEM) and electron probe microanalysis (EPMA) techniques were used to continue characterization of the microstructure of NO_x trap catalysts and oxidation catalysts. In the previous report, the microstructure and chemistry of samples from Reactor II (platinum loading ~2 wt %) at different positions along the reactor were studied, and the changes in morphology of platinum particles as well as the distribution of elements such as the trapping component within the washcoat were elucidated. Subsequently, a variety of both NO_x trap catalysts and oxidation catalysts were examined to quantify the precious metal particle size distributions both as a function of aging as well as macroscopic position in the reactor. In addition, the location and structure of the BMO trapping component of the NO_x trap systems were determined. Some example results and main conclusions from the microscopy experiments are given below.

The platinum particles of a fresh Pt/Ba/ γ -alumina model catalyst sample were examined. The sample had a target loading of 1.6 g/in.³ and was exposed to 500°C in its preparation. The majority of platinum particles were observed to be between 1 and 2 nm in size, as can be seen in Figure 6. The HA-ADF STEM image has bright contrast for heavy elements, while lighter elements appear darker. The particles were too fine for quantification via image processing. “Spectral imaging” is an advanced technique for elemental analysis in electron beam instruments whereby a full EDS spectrum from 0–20 keV is collected at every individual pixel location. The collected data can be manipulated off-line to generate 1-dimensional and

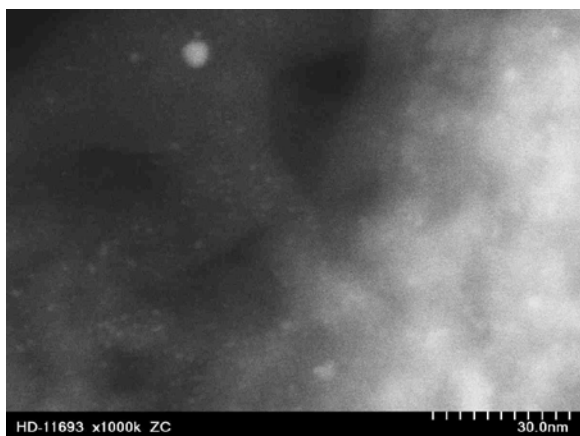


Figure 6. HA-ADF (Z-contrast) STEM image of platinum particles on alumina washcoat in sample PBA1. The majority of the particles are 1–2 nm in diameter in this micrograph.

2-dimensional elemental line scans and maps. Figure 7 shows both the HA-ADF STEM image and an extracted barium X-ray map for the sample. The X-ray map conclusively shows the spatial distribution of the barium-containing phase in this sample, and comparison with the high angle-annular dark field (HA-ADF) image allows for the identification of barium containing areas relative to the morphology and brightness seen in the HA-ADF image. Samples containing Pt/BMO/ γ -alumina were also examined. Spectral imaging identified the trapping component as BMO-based. As seen in Figure 8, the BMO phase is widely distributed but not as easily identified from just the HA-ADF images.

Unlike previous specimens, sample D (see X-ray section above) came as a much longer core

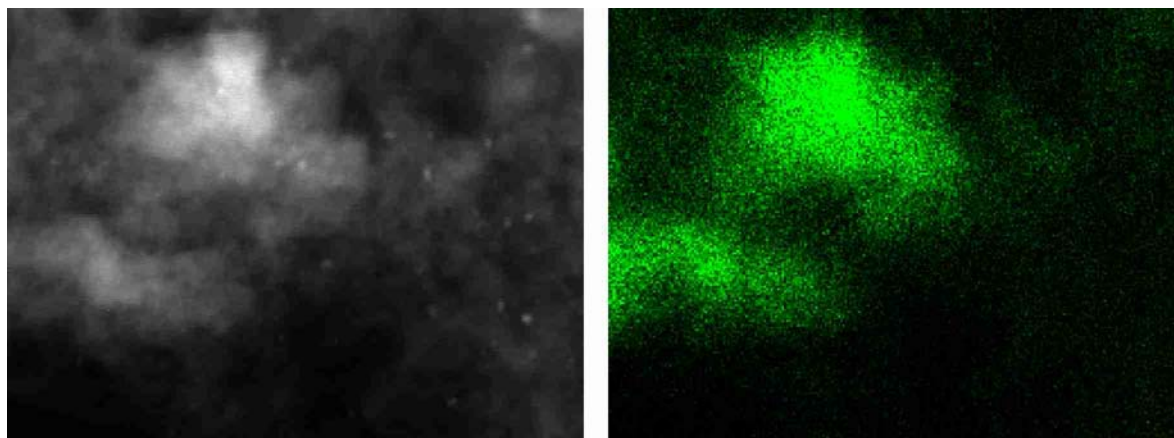


Figure 7. (a) HA-ADF STEM image. (b) Barium X-ray map extracted from spectral image. Barium containing phase corresponds to the large bright area in (a).

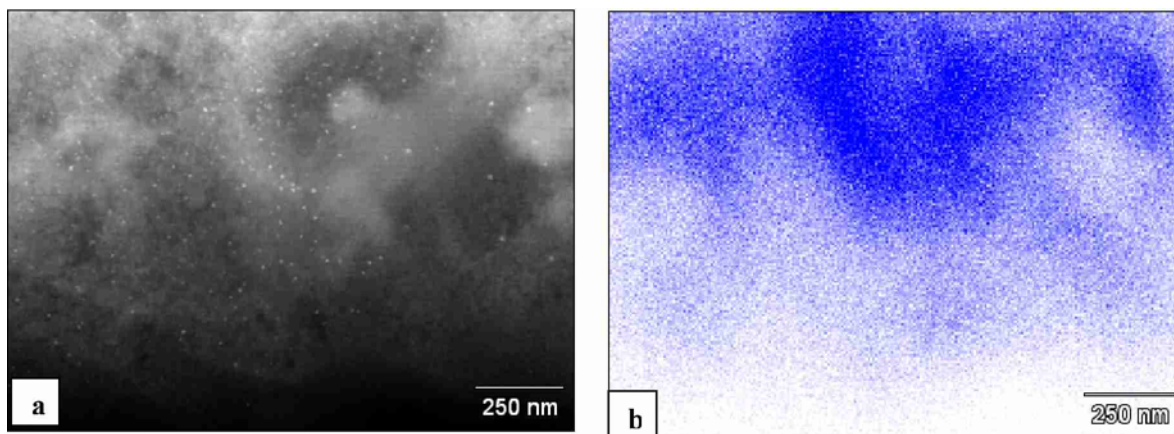


Figure 8. (a) HA-ADF STEM image. (b) BMO X-ray map. There has been some uncompensated shift between the reference image and the map. The BMO phase is widely distributed, but not easily identified in the HA-ADF image alone (a).

with the request to analyze the platinum particle size distribution down the length of the monolith. Sample D1 was taken near the smooth/flat upstream face of the monolith [see left side of inset in Figure 3(b)] and was closer to the engine. Sample D2 was from an area 7 cm away along the length of the monolith, near the rough/jagged side. Figure 9 shows the comparison of the platinum particle size distributions for samples D1 and D2. Sample D1 exhibits a very typical Gaussian distribution of particle sizes, while sample D2 has a bimodal distribution with both a population of small catalyst particles and large catalyst particles. For 757 particles in

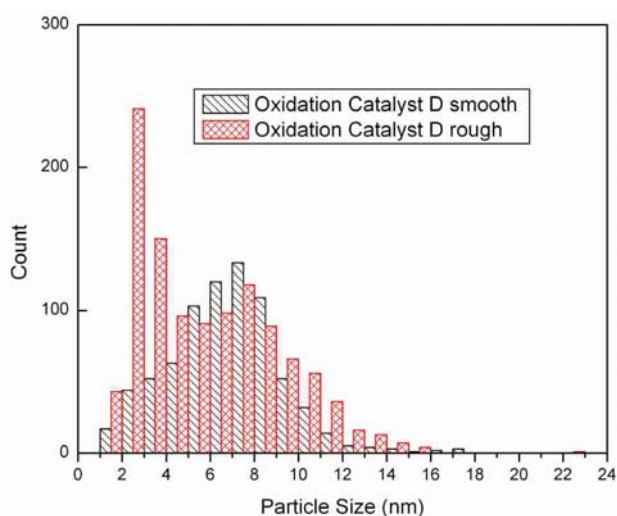


Figure 9. Comparison of platinum particle size distributions from two different areas on the same monolith. Each distribution is based on ten images each.

D1, the median and mean particle sizes were 6.82 and 6.76 nm, respectively. For 1125 particles in D2, the median and mean particle sizes were 5.87 and 5.48 nm, respectively. The higher temperatures that the platinum particles at location D1 experienced appear to have coarsened the particle slightly.

References

1. R-S. Zhou and R. L. Snyder, "Structures and Transformation Mechanisms of the η , γ and θ Transition Aluminas," *Acta Cryst.*, **B47**, 617–30 (1991).

Presentations and Publications

T. R. Watkins, L. Allard, D. Blom, M. J. Lance, H. Meyer, L. Walker, C. Narula, R. D. England, B. Epling, H. Fang, and T. Yonushonis, "Development of Materials Analysis Tools for Studying NO_x Adsorber Catalysts," [Revised] presented at 11th Diesel Engine Emission Reduction (DEER) Conference, Chicago, Illinois, August 24, 2005.

T. R. Watkins, L. Allard, D. Blom, M. J. Lance, C. Narula, H. Meyer, R. D. England, H. Fang, T. Yonushonis, and H. Hess, "Catalyst Characterization, CRADA No. ORNL-02-0659 with Cummins, Inc.," presented at the Heavy Vehicle Materials Program Review, Oak Ridge National Laboratory, Oak Ridge, Tennessee, September 14, 2005.

H. L. Fang, M. J. Lance, and G. S. Painter, "Raman Characterization of Pt-support Interactions on Metal Oxides," in preparation.

